Impacts of Different Charging Strategies on the Electric Vehicle Battery Charger Circuit Using Phase-Shift Full-Bridge Converter

Lyu, Dingsihao; Soeiro, Thiago Batista ; Bauer, Pavol

DOI
10.1109/PEMC48073.2021.9432497

Publication date
2021

Document Version
Final published version

Published in
Proceedings - 2021 IEEE 19th International Power Electronics and Motion Control Conference, PEMC 2021

Impacts of Different Charging Strategies on the Electric Vehicle Battery Charger Circuit Using Phase-Shift Full-Bridge Converter

Dingsihao Lyu
Delft University of Technology
Delft, The Netherlands
d.lyu@tudelft.nl

Thiago Batista Soeiro
Delft University of Technology
Delft, The Netherlands
t.batistasoeiro@tudelft.nl

Pavol Bauer
Delft University of Technology
Delft, The Netherlands
p.bauer@tudelft.nl

2021 IEEE 19th International Power Electronics and Motion Control Conference (PEMC) | 978-1-7281-5660-6/20/$31.00 ©2021 IEEE | DOI: 10.1109/PEMC48073.2021.9432497

***Abstract*—This paper compares the influences of two different charging strategies on the performance of the Electric Vehicle (EV) charging system, including the EV battery, the Battery Management System (BMS), and the power electronic converter. Firstly, the two types of EV charging strategies are explained. Herein, the characteristics, the influences on the EV battery, and the respective requirements for the hardware and communication of the BMS and power electronic converter are summarized. Secondly, a simulation case study is conducted to investigate the influences of the two charging strategies on the performance of a typical power electronic converters employed as a back-end converter of a fast EV charger. A modular 50kW DC-DC EV charger constructed with five parallel-connected 10kW Phase-Shift Full-Bridge (PSFB) DC-DC converter is modelled with two different charging strategies, and two comparison metrics are proposed for a benchmark: the charging-cycle efficiency and the installation utilization rate. The results show that these two comparison metrics are influenced by the charging strategies of the EV.**

***Index Terms*—electric vehicles (EVs), EV charger, charging strategy, charging profile, phase-shift full-bridge converter, DC-DC converter**

I. Introduction

As the Electric Vehicle (EV) market grows rapidly, the demand for fast and efficient battery charging services also increases. In order to meet this need, battery technology research aims to push the limits for fast charging from multiple fronts, including the electrolyte and electrode materials, material architectures, and cell to pack design [1] [2].

While the EV battery and the charger are two of the most important components in the EV charging process from the energy transfer perspective, the implemented charging strategies, which define the way how the electric energy is transferred from the charger to the EV battery, also have significant impacts on the whole performance metrics of the system. The charging strategy results to certain voltage and current profile during the EV charging process, denoted here as charging profile. On the one hand, the charging profile, especially the injected current, determines how fast the battery is being charged, and it affects the efficiency and aging of the cells. On the other hand, it determines how and in what range the power electronics converter of the EV charger will operate, thus affecting the efficiency and utilization rate of the circuit components. Moreover, the charging strategies require different monitoring and control methods for the power converter as well as the Battery Management System (BMS).

The standard charging strategy is the Constant Current-Constant Voltage (CC-CV) due to its simplicity and ease implementation [3]. Besides CC-CV, alternative charging strategies have been proposed and/or comparative experiments were conducted in [4] - [16]. These techniques may have multiple purposes, such as, to shorten the charging time without bringing detrimental influence on the battery lifetime, to increase the charging efficiency and/or to improve the battery capacity. Above all, the focuses of those studies were on the impacts of different charging strategies on the battery cells. The work in [1] provides an overview of charging strategies, including a summary of different experimental results from the literature. However, it misses their impacts on the BMS and power electronics. In [2] a summary of the implementation requirements for different charging strategies is given, however, the impact on the power electronics converter is not qualitatively investigated. Table I summarized the defining parameters, the impacts on the battery, the requirements for the BMS and the charger of the charging strategies. The influences on the battery are based on the experimental results from various publications as indicated in Table I, and the requirements for the BMS and the charger are based on the defining parameters of the charging strategies.

In order to obtain a more in-depth understanding of the impacts of the charging strategies on the EV charger circuit, a simulation case study is conducted in this paper. Firstly, two charging strategies, the CC-CV and Multi-Step Constant Current Constant Voltage (MSCC-CV) are reviewed. Then, the impacts of the two charging strategies on the power electronic converters is investigated by the simulation of a Phase Shift Full Bridge (PSFB) DC-DC converter, which is a conventional circuit solution employed in DC-type fast EV chargers.

These two strategies are chosen in order to achieve a fairer comparison, since they have the same requirements for the

This research has been funded within the Power2Power project, which is a European co-funded innovation project on Semiconductor Industry. The project receives grants from the European H2020 research and innovation program, ECSEL Joint Undertaking, and National Funding Authorities from eight involved countries under grant agreement No. 826417. The participating countries are Austria, Finland, Germany including the Free States of Saxony and Thuringia, Hungary, the Netherlands, Slovakia, Spain and Switzerland.

	CC-CV	MSCC	Boost Charging	Pulse Charging
Defining Parameters	I_{CC}, I_{end}, V_{max}	$I_{CC,n}$ $(1 \leq n \leq N)$, V_{MSCC}	$I_{b(max)}$, I_{CC}, I_{end}, $V_{b(max)}$, V_{max}	I_{CC}, V_{max}, V_{PC}
Impacts on the Battery	/	1. shorter charging time [11] 2. higher charging efficiency [11] [17] 3. longer cycle life [11] [17]	1. shorter charging time [4] [12] [16]	1. reduced charging time [10] 2. higher capacity utilization [10] 3. longer cycle life [10]
		4. prolonged charging time [16]	2. shorter cycle life [16]	4. prolonged charging time [16] 5. lower capacity utilization [16]
Requirements for the BMS	1. current sensing 2. voltage sensing	1. current sensing 2. voltage sensing	1. current sensing 2. voltage sensing 3. timer functionality	1. current sensing 2. voltage sensing 3. timer functionality
Requirements for the charger	1. voltage control 2. current control	1. current control	1. voltage control 2. current control 3. extra power capacity	1. current control

TABLE I: The defining parameters of the charging profiles, and their impacts on the battery, requirements for the BMS and the charger. Note that the impacts on the battery are presented as compared to the CC-CV charging strategy

hardware of the BMS and charger, and similar performance regarding the battery and the charging process, when the charging current rate of the initial CC phase and the termination current rate are selected to be the same. The Boost Charging strategy is not considered because the high current charging in the beginning requires a higher power capability of the charger compared to the other strategies, making the comparison inequitable. The Pulse Charging (PC) strategy is not considered because the current pulse is not practically acceptable without a large energy buffering device, such as a inner battery storage. Without a large energy buffer, PC will have a detrimental impact on the grid power quality caused by the intermittent power demand.

II. REVIEW OF BATTERY CHARGING STRATEGIES

A. Constant Current-Constant Voltage (CC-CV)

The CC-CV charging strategy features a two-stage charging process. Figure 1a shows the illustration of the resulted charging profile for CC-CV.

In the first stage, the battery is charged by a controlled constant current with a current rate of I_{CC}. I_{CC} can be set to be any current value allowed by the EV battery as long as it does not exceed the current limitation of the charger. In general, a higher current rate during the CC phase will result in reduced charging time. However, the gain in time would become smaller as the current rate becomes too higher due to the necessary extension of the following CV phase to reach the same final State-of-Charge (SoC) [1]. Moreover, detrimental effects to the battery may occur with high current rate, leading to the shortening of the battery cells' cycle-life [1]. The CC charging period ends when the cell voltage reaches a voltage limit V_{max}, which can be equal to the maximum voltage of the individual cell V_{cutoff} (typically $4.2V - 4.4V$ per cell, depending on the battery chemistry), and it can also be set to be lower than V_{cutoff} due to safety and to strategically extend the battery cycle-life [16]. Following that, the CV charging period begins, where the charging voltage is kept constant at V_{max} while the current injected into the battery gradually decreases. The whole charging process ends when the current falls to I_{end}. Note that the CV phase allows for the concentration gradients within the electrode particles to disperse and is usually necessary to obtain high capacity utilisation without exceeding the maximum voltage [1].

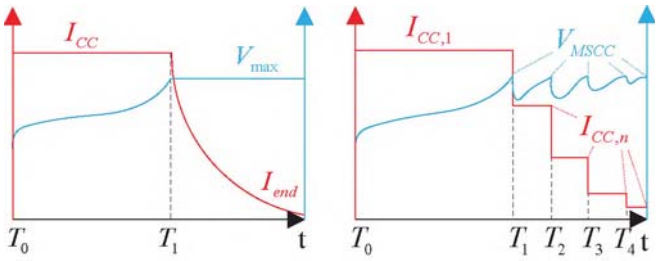

(a) CC-CV (b) MSCC

Fig. 1: Illustrations of EV battery charging profiles

B. Multi-Step Constant Current

Multi-Step Constant Current strategy was proposed in [7] [8] as an alternative strategy that shortens the charging time, improves energy efficiency, and prolongs the cycle-life of valve-regulated lead/acid and Ni/MH batteries. It has been later applied to Li-ion batteries, and similar benefits were observed [11]. Figure 1b shows the MSCC charging profile.

MSCC is composed by $N \times$ CC phases, where N is the number of current steps. Similarly to the standard CC-CV strategy, MSCC begins the charging with a constant current $I_{CC,1}$ until the battery voltage reaches the voltage limit V_{MSCC}. Then instead of switching into a CV phase, the charging current decreases to the second step with the value $I_{CC,2}$, leading to a voltage drops below V_{MSCC}, allowing the battery to be further charged at CC. Once the battery voltage reaches the limit V_{MSCC} again, the next step takes place with another reduced current level. The charging process is terminated when V_{MSCC} is reached at the set lowest current stage $I_{cc,N}$.

A CV charging stage characterized by V_{max} and I_{end} can be added at the end of the lowest current stage in order to have better capacity utilization of the battery. This modified MSCC is denoted as MSCC-CV, and is very similar to the CC-CV charging strategy.

III. Impacts of Charging Strategies on the Performance of a PSFB Converter

The different charging strategies will particularly influence the overall efficiency of the charger. This occurs because power electronic converters usually have a limited operation range in which the efficiency is optimal. Therefore, it is preferable to choose a charging strategy that matches, as long as possible, the converter operation within this optimal range.

The utilization rate of the charger's power capability is also affected by the charging strategies. By implementing a charging strategy that involves a long partial load operation, the charger will deliver only a fraction of its power capability.

In order to understand how would different charging strategies influence the performance of the EV charger, a 50kW DC-DC EV charger, which is constructed by paralleling five 10kW DC-DC phase-shift full-bridge power modules, is modelled with two different charging strategies, i.e., the CC-CV and the MSCC-CV.

A. PSFB Analytical Modeling

The PSFB is a popular isolated DC-DC topology for medium to high power applications. This is mainly because of the simple structure, controllable current source behaviour, good efficiency and reduced EMI emission enabled by the Zero Voltage Switching (ZVS) capability. Figure 2 shows the basic schematic of the PSFB converter.

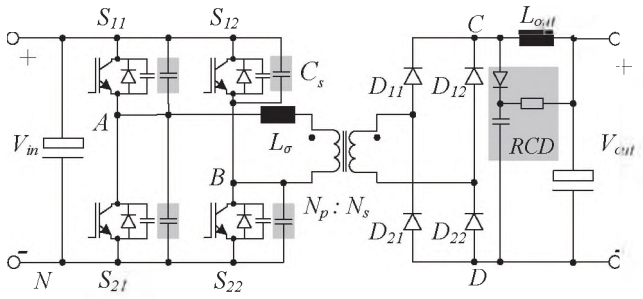

Fig. 2: The schematic of the PSFB converter including the RCD snubber and the optional turn-off snubber capacitors C_s marked in gray boxes

The PSFB converter consists of a full-bridge inverter, a high-frequency isolation transformer with an equivalent leakage inductance L_σ referred to the primary-side and a diode-bridge rectifier on the secondary side, and a second-order low-pass output passive filter consisting of L_{out} and C_{out}. Note that the diode-bridge rectifier are sometimes replaced by a synchronous rectifier using unipolar transistors for reducing conduction losses. The optional lossless snubber capacitors C_s at the full-bridge are for reducing turn-off switching losses (but it will narrow the ZVS turn-on range), and a RCD snubber circuit is used at the secondary-side between the terminal C and D to clamp the voltage across the rectifier.

The PSFB is typically controlled with fixed switching frequency by phase-shift modulation where the two half-bridge legs are operated with 50% duty cycle. The phase-shift refers to the asynchronization between the operation of the two half-bridge legs. When the phase shift is null, the diagonal pair of transistors (S_{11} & S_{22}, or S_{12} & S_{21}) turn on and off synchronously, making the primary side voltage v_{AB} alternate between $+V_{in}$ and $-V_{in}$, which is equivalent to a bipolar modulation. When the phase shift is non-null, the synchronization is broken, and the parallel pair of transistors (S_{11} & S_{12}, S_{21} & S_{22}) are able to be kept turned on at the same time, creating a third circuit state that is $V_{AB} = 0V$, leading to a controllable unipolor modulation action. Due to the impressed i_p caused by the energy stored in L_σ and the necessary permute of charges between the inverter bridge capacitances the switching transition in each half-bridge leg creates a lowered di_p/dt and dV_{AB}/dt on the primary side. If there is enough energy stored in L_σ to complete the permutation of charges across the bridge capacitance the ZVS turn-on of the transistors become possible.

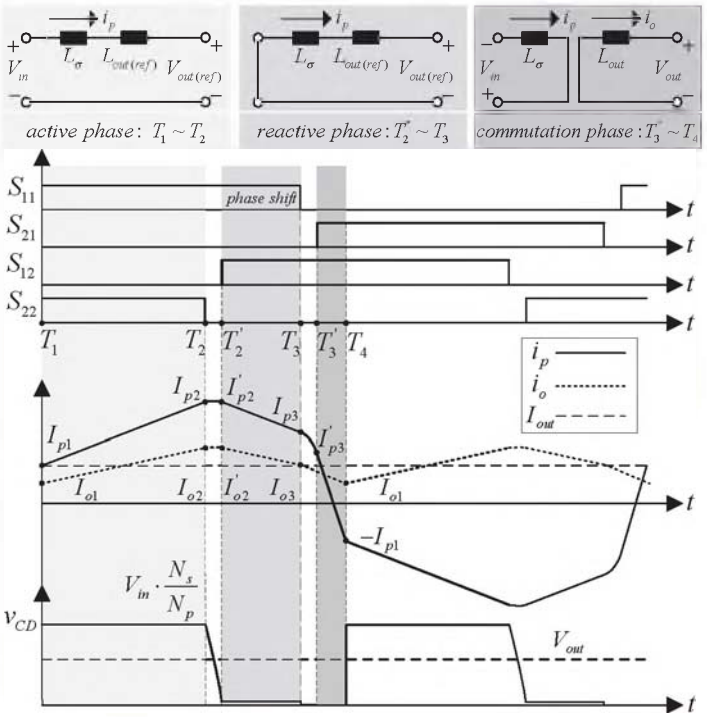

Fig. 3: Operational waveform of the PSFB converter and the equivalent circuits with the secondary side reflected to the primary side

Figure 3 shows the typical operational waveforms of the PSFB converter and the equivalent circuits during the normal operation. The operation can be divided into 5 phases: the active phase where the diagonal transistors conduct; the reactive phase where the parallel transistors conduct; the commutation phase where the secondary side current commutes among the rectifier diodes; and two transition phase during the dead-time of each bridge. A complete description of the operation of a PSFB converter can be found in [21].

For the simplicity of circuit analysis, the assumption is made that $T_2 = T_2'$, $T_3 = T_3' = T_4$, $I_{p2} = I_{p2}'$, and $I_{p3} = I_{p3}' = I_{p1}$. This is valid because the transition and commutation phases

are relatively very short compared to the other two phases, thus their influences on the overall current waveform are small. The current values in Fig 3 could be calculated as followings.

$$I_{o1} = I_{o3} = \frac{P}{V_{out}} - \frac{D_{eff}(V_{in(ref)} - V_{out})}{4f_{sw}(L_{\sigma(ref)} + L_{out})} \tag{1}$$

$$I_{o2} = I_{o1} + \frac{D_{eff}(V_{in(ref)} - V_{out})}{2f_{sw}(L_{\sigma(ref)} + L_{out})} \tag{2}$$

$$I_{p1,2,3} = \frac{I_{o1,2,3}}{n} \tag{3}$$

where D_{eff}, $V_{in(ref)}$ and $L_{\sigma(ref)}$ are the effective duty cycle, the reflected input voltage on the secondary side, and the reflected leakage inductance on the secondary side. They can be calculated as:

$$D_{eff} = 2 \cdot (T_2 - T_1)/T \tag{4}$$

$$V_{in(ref)} = \frac{V_{in}}{n} \tag{5}$$

$$L_{\sigma(ref)} = \frac{L_\sigma}{n^2} \tag{6}$$

The current waveform, rms and average current stresses for each components can be obtained based on these current values. The following equations show the rms and average current for the IGBT, the body diode BD, and the secondary side rectifier diodes D.

$$I_{rms(IGBT,leading)} = \sqrt{\frac{D_{eff}(I_{p1}^2 + I_{p1}I_{p2} + I_{p2}^2)}{6}} \tag{7}$$

$$I_{rms(IGBT,lagging)} = \sqrt{\frac{I_{p1}^2 + I_{p1}I_{p2} + I_{p2}^2}{6}} \tag{8}$$

$$I_{avg(IGBT,leading)} = \frac{D_{eff}(I_{p1} + I_{p2})}{4} \tag{9}$$

$$I_{avg(IGBT,lagging)} = \frac{I_{p1} + I_{p2}}{4} \tag{10}$$

$$I_{rms(BD,leading)} = \sqrt{\frac{(1 - D_{eff})(I_{p1}^2 + I_{p1}I_{p2} + I_{p2}^2)}{6}} \tag{11}$$

$$I_{avg(BD,leading)} = \frac{(1 - D_{eff})(I_{p1} + I_{p2})}{4} \tag{12}$$

$$I_{rms(BD,lagging)} = I_{avg(BD,lagging)} = 0 \tag{13}$$

$$I_{rms(D)} = \sqrt{\frac{I_{s1}^2 + I_{s1}I_{s2} + I_{s2}^2}{6}} \tag{14}$$

$$I_{avg(D)} = \frac{I_{s1} + I_{s2}}{4} \tag{15}$$

B. PSFB Semiconductor Loss Model

A 10kW PSFB converter is modeled to evaluate the semiconductor losses with different charging strategies. The circuit parameters and the range of operation conditions are listed in Table II.

Circuit Parameters				Operation Conditions			
N_p/N_s	L_σ	L_{out}	C_s	f_{sw}	V_{in}	V_{out}	P
1.235	$10\mu H$	$0.487mH$	$10.7nF$	15kHz	640V	200-500V	0-10kW

TABLE II: Specifications of the 10kW PSFB converter

For the full-bridge the IGBT *IKW40N120CS6XKSA1* from Infineon is used, while the output diode-bridge employs the SiC diode *C4D15120A* from Wolfspeed/Cree.

The losses on the IGBT, the body diode of the IGBT, and the rectifier diodes consist of conduction and switching loss. The conduction loss can be calculated as a sum of an equivalent on-resistance loss and a forward voltage drop loss, as:

$$P_{c(IGBT/BD/D)} = I_{rms(IGBT/BD/D)}^2 \cdot R_{on(IGBT/BD/D)} + I_{avg(IGBT/BD/D)} \cdot V_{F(IGBT/BD/D)}$$

The on-state resistance R_{on} and the forward voltage drop V_F For the IGBT, the body diode BD and the rectifier diodes D can be obtained from their typical on-state characteristic as stated in their datasheets, and they are listed in Table III.

The switching loss of each IGBT is the sum of the turn-on and the turn-off losses:

$$P_{sw(I)} = E_{on} \cdot f_{sw} + E_{off} \cdot f_{sw} \tag{16}$$

where the turn-on and the turn-off losses can be calculated based on the measured switching energy loss by double-pulse testing (DPT) and the ZVS condition as:

$$E_{off} = E_{off(DPT)} - E_{oes} - E_{snb} \tag{17}$$

$$\begin{cases} E_{on(DPT)} = 0, & if \text{ ZVS=true} \\ E_{on} = E_{on(DPT)} + E_{oes} + E_{snb}, & if \text{ ZVS=false} \end{cases} \tag{18}$$

$E_{off(DPT)}$ and $E_{on(DPT)}$ is the measured switching energy loss of the IGBT, which is shown in Figure 4. E_{oes} is the stored energy in the equivalent instrinsic output capacitor C_{oes} of the IGBT and diode, and E_{snb} is the stored energy in the optional lossless turn-off snubber capacitor C_s. E_{oes} and E_{snb} can be roughly estimated respectively as:

$$E_{oes} = \frac{1}{2} \cdot C_{oes} \cdot V_{in}^2 \tag{19}$$

$$E_{snb} = \frac{1}{2} \cdot C_s \cdot V_{in}^2 \tag{20}$$

The switching loss of the diode consists of the reverse recovery loss which is relatively low in SiC diodes:

$$P_{sw(D)} = k \cdot Q_c \cdot (V_{in} \cdot \frac{N_s}{N_p}) \cdot f_{sw} \tag{21}$$

The Q_c is the reverse recovery energy loss given in the Diode datasheet. C_{oes} and Q_c are listed in Table III.

components	characteristics	values
IKW40N120CS6XKSA1 (IGBT)	C_{oes}	130pF
	$R_{on(IGBT)}$	28.100mΩ
	$V_{F(IGBT)}$	1.217V
IKW40N120CS6XKSA1 (body diode)	$R_{on(BD)}$	21.900mΩ
	$V_{F(BD)}$	1.501V
C4D15120A	$R_{on(D)}$	74.806mΩ
	$V_{F(D)}$	0.795V
	$Q_{c(D)}$	65nC
	k	0.667

TABLE III: electrical characteristics of the used components

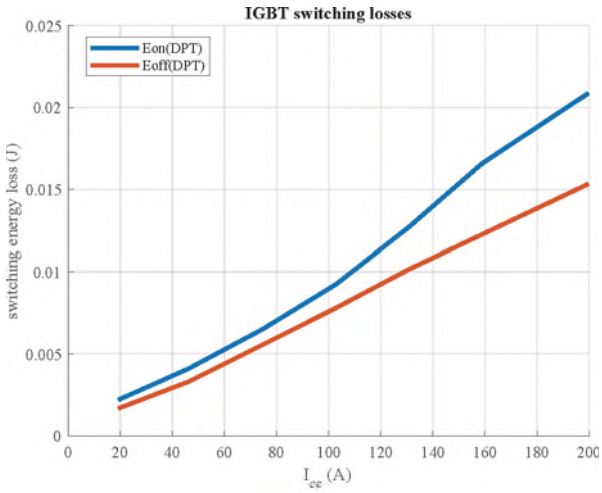

Fig. 4: the measured switching energy loss of the IGBT

With the analytical model and the loss calculation, The efficiency map of the converter that visualizes the efficiency at each operation condition is shown in Figure 5.

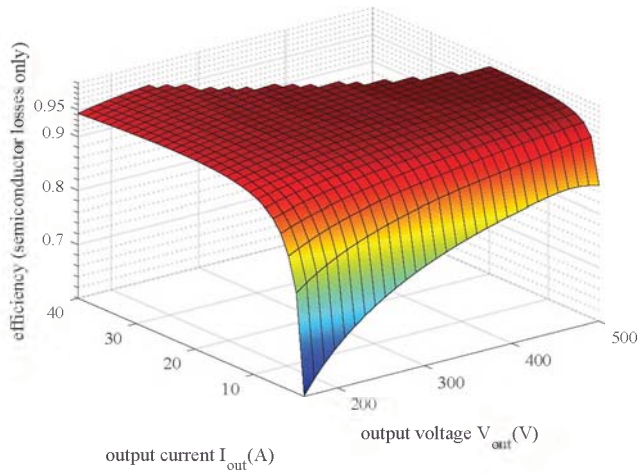

Fig. 5: The efficiency map for the 10kW PSFB converter considering only the semiconductor losses

C. Charging Profile Simulation

In order to obtain the charging profile for the CC-CV and MSCC-CV strategies, an impedance-based model of a lithium nickel oxide (LNCO) Boston Power SWING 5300 given in [18], [20] is used. The model is constructed by series connected impedance blocks, which is derived from a specific electrochemical equation linked to the battery operation.

Two sets of comparison simulations with different current rates are conducted. The characteristics of the CC-CV and MSCC-CV charging strategies of the two sets of simulations are listed in Table IV. For a fair comparison, in each simulation, I_{CC} of the CC-CV and $I_{CC,1}$ of the MSCC-CV are set to be the same. Moreover, V_{max} and V_{MSCC}, and I_{end} are set to be equal as well.

For comparison I, a battery pack with 44.5kWh nominal energy capacity, and 350V nominal battery voltage is simulated based on the cell model mentioned before. These battery specifications are similar to those of a Nissan Leaf.

For comparison II, the energy capacity is reduced to 22.2kWh, while keeping the battery rated voltage of 350V. This is to ensure that the actual charging current of comparison II is similar to that of comparison I, despite the current rate is doubled. These battery specifications are similar to those of a BMW i3 60Ah model.

IV. Benchmarking Results

A. Comparison I: 1C current rate

Figure 6a and 6b show the CC-CV and MSCC-CV charging and power profiles with 1C current rate for the 5 parallel 10kW power modules. Assumption is made that the power modules are always operating at full power if possible.

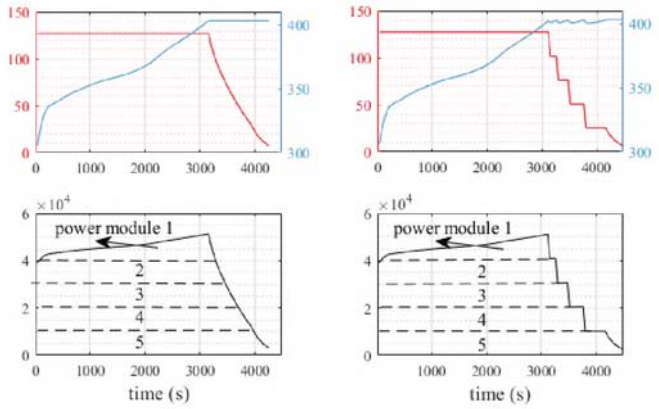

(a) CC-CV (b) MSCC-CV

Fig. 6: The charging and power profiles for a 44.5kWh EV battery with 1C current rate. The red line is the charing current(A), the blue line is the charging voltage (V), and the black line is the charging power (W)

It can be seen that since I_{CC} and $I_{CC,1}$ are set to be the same, the initial CC phase of the two charging strategies are identical. While in the CV phase of the CC-CV strategy, the power modules operates in partial load condition defined by the current drop as shown in Figure 6a. Conversely, the MSCC-CV strategy mimics the partial load operation by

	battery specifications		CC-CV characteristics			MSCC-CV characteristics				
	nominal capacity	nominal voltage	I_{CC}	V_{max}	I_{end}	N	$I_{CC,n}$	V_{MSCC}	V_{max}	I_{end}
comparison I	44.5kWh	350V	$1C$	$4.2V$	$0.05C$	5	$1C/n$	$4.2V$	$4.2V$	0.05C
comparison II	22.2kWh	350V	$2C$	$4.2V$	$0.05C$	5	$2C/n$	$4.2V$	$4.2V$	0.05C

TABLE IV: the specifications of the battery and the two charging strategies used in the two comparison experiments

turning off one-by-one the paralleled power modules once the charging voltage reaches V_{MSCC}, as shown in Figure 6b.

As for the individual power modules, in the case of CC-CV charging strategy, the power modules 2-5 are operating in a Constant-Power Constant-Voltage (CP-CV) manner, while the power module 1 is operating in a Various-Power Constant-Voltage (VP-CV) manner. While in the case of MSCC-CV charging strategy, the power modules 2-4 are always operating at Constant-Power (CP), whereas module 1 is at Various-Power (VP), and module 5 is at CP-CV. This not only means the operation range of power modules 1-4 with the MSCC-CV charging strategy are narrowed compared to the CC-CV strategy, but also that each operating module have a higher power utilization.

Two quantitative indicators are suggested for comparison purpose, the charging cycle efficiency, and the utilization rate of the installed power. The charging cycle efficiency is the overall efficiency considering the whole operation range of the charging process. It can be calculated as eq. (22), where n is the indicator of the power modules, T_n is the operation time of the power module n, $P_n(t)$ is the charging power of the power module n, and $P_{loss,n}(t)$ is the power loss of the power module n.

$$\eta_{cycle} = \frac{\sum_{n=1}^{n=5} \int_0^{T_n} (P_n(t) - P_{loss,n}(t)) \cdot dt}{\sum_{n=1}^{n=5} \int_0^{T_n} P_n(t) \cdot dt} \tag{22}$$

The utilization rate of the installed power is the indicator that shows how efficient is the installed power been used. The higher the utilization rate, the longer that converter operates in the rated power within a certain period. It can be calculated as eq. (23), where $T_{full,n}$ is the time of operation at rated or higher power in the total operation time of the module n.

$$\nu = \frac{\sum_{n=1}^{n=5} T_{full,n}}{\sum_{n=1}^{n=5} T_n} \tag{23}$$

The charging cycle efficiency and the utilization rate of the installed power are calculated for the CC-CV and MSCC-CV charging profile of comparison I and listed in Table V.

It can be seen from Table V that, the two charging strategies result in the charging cycle efficiency. This will be interpreted later together with the result of comparison II. Secondly, the utilization rate of the installed power of the MSCC-CV

	CC-CV	MSCC-CV
charging cycle efficiency η_{cycle}	97.51%	97.51%
utilization rate of installed power ν	78.97%	82.90%

TABLE V: The simulation results of comparison I

charging strategy, 82.90%, is 3.93% higher than that of the CC-CV strategy, which is 78.97%. This is due to the fact that the MSCC-CV strategy turns off the power modules rather than trying to operate each one with lower power. This higher utilization rate of the installed power can be utilized to provide more accessible charging service if the power modules are combined together in a flexible way, in which individual power module has its own output. In this way, once a power module is turned off during a charging service, it can be used to provide another charging service, such as feeding power to another EV, thus the accessibility of a charging station is increased.

B. Comparison II: 2C current rate

Figure 7a and 7b show the CC-CV and MSCC-CV charging and power profiles with 2C current rate for the 5 power modules respectively.

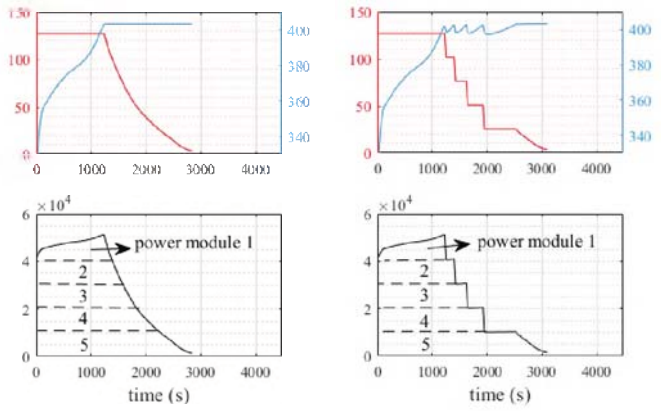

(a) CC-CV (b) MSCC-CV

Fig. 7: The charging and power profiles for a 22.2kWh EV battery with 2C current rate. The red line is the charging current (A), the blue line is the charging voltage (V), and the black line is the charging power (W)

Compared to figure 6a and 6b, it can be seen that in the charging profiles with 2C current rate, the percentage of the CV phase compared to the CC phase is much longer, this makes the percentage of time operating at lower power condition higher. This is due the electrochemical reactions of the battery cells.

The charging cycle efficiency and the utilization rate of the installed power are calculated for the CC-CV and MSCC-CV charging profile of comparison II and listed in Table VI.

	CC-CV	MSCC-CV
charging cycle efficiency η_{cycle}	97.63%	97.65%
utilization rate of installed power ν	72.92%	82.21%

TABLE VI: The simulation results of comparison II

It can be seen that the charging cycle efficiencies for CC-CV and MSCC-CV strategies are both slightly higher than that of comparison I, and at the same time, the one of the MSCC-CV is 0.02% higher than that of the CC-CV. All these differences of charging cycle efficiency can be explained by the efficiency performance of the converter at different operation conditions as shown in Figure 8.

Figure 8 shows the efficiency map of the converter together with the CP-CV operating trajectory. It can be seen from Figure 8 that, as the converter operates following the CP-CV trajectory, the instantaneous power efficiency of the converter will increase during the CP phase, and it will reaches the peak in the beginning of the CV phase, and then starts dropping in the rest of the CV phase. The fact that the power efficiency is the highest at the end of CP phase and the beginning part of CP phase indicates that the MSCC-CV strategy which operates the parallel converters mostly in the CP phase, as shown in Figure 6b, does not necessarily bring higher charging cycle efficiency, compared to the CC-CV strategy which involves longer partial load operation in the CV phase as shown in comparison I,

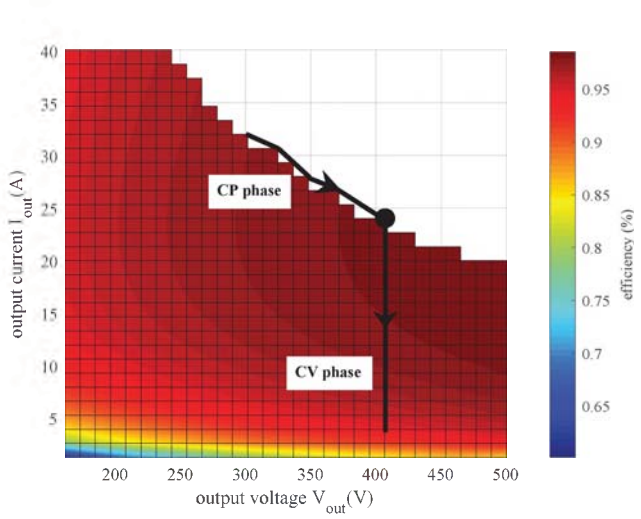

Fig. 8: The efficiency map of the power module with the trajectory of the CP-CV charging profile

The utilization rate of the installed power for MSCC-CV with an initial current rate of 2C, 82.21%, is 9.29% higher than that of CC-CV, which is more than 2 times than the difference found in comparison I. This is due to the larger percentage of CV phase within the whole charging process with 2C current rate.

V. Conclusion

Firstly, different charging strategies might or might not lead to different charging cycle efficiency on the same power electronic converter, depending on the composition of the charging profile and the power efficiency performance of the converter on the charging profile. Charging strategies such as MSCC-CV together with the modular structure of the charger, can narrow the operation range of the converter compared to the CC-CV. However, smaller operation range does not necessarily guarantee higher charging cycle efficiency, as demonstrated by the comparison results in this paper. Further research can investigate the forming factors of the efficiency map of the converter, and the ways to reshape it to provide better charging cycle efficiency with different charging strategies.

Secondly, different charging strategies lead to different utilization rate of installed power. This is due to the mechanism of how different charging strategies controls the charging process. For MSCC-CV or MSCC, the power modules are turned off from full power operation once the voltage has reached the set limits, rather than operated in partial power as in CC-CV, and this greatly improves the utilization rate of the installed power if combined with a flexible parallel modular multiple outputs structure. And this higher utilization rate would bring better accessibility to the EV charging stations.

Therefore, alternative charging strategies other than CC-CV, such as MSCC-CV, can improve the performance of the power electronic converters of the EV chargers in terms of charging cycle efficiency and utilization rate of the installed power, if the converters' efficiency maps match with them, and a flexible structure of the power modules is implemented. Last but not least, as the charging current rate increase, the space of improvement for the charging cycle efficiency and utilization rate of the installed power will be larger, because the time of operating at partial power is longer.

References

[1] A. Tomaszewska et al., "Lithium-ion battery fast charging: A review," eTransportation, vol. 1, p. 100011, 2019/08/01/ 2019, doi: https://doi.org/10.1016/j.etran.2019.100011.

[2] C. Chen, F. Shang, M. Salameh, and M. Krishnamurthy, "Challenges and Advancements in Fast Charging Solutions for EVs: A Technological Review," in 2018 IEEE Transportation Electrification Conference and Expo (ITEC), 13-15 June 2018 2018, pp. 695-701, doi: 10.1109/ITEC.2018.8450139.

[3] D. U. Sauer, "BATTERIES — Charge–Discharge Curves," in Encyclopedia of Electrochemical Power Sources, J. Garche Ed. Amsterdam: Elsevier, 2009, pp. 443-451.

[4] D. Anseán, M. González, J. C. Viera, V. M. García, C. Blanco, and M. Valledor, "Fast charging technique for high power lithium iron phosphate batteries: A cycle life analysis," Journal of Power Sources, vol. 239, pp. 9-15, 2013/10/01/ 2013, doi: https://doi.org/10.1016/j.jpowsour.2013.03.044.

[5] L. Chen, "Design of Duty-Varied Voltage Pulse Charger for Improving Li-Ion Battery-Charging Response," IEEE Transactions on Industrial Electronics, vol. 56, no. 2, pp. 480-487, 2009, doi: 10.1109/TIE.2008.2002725.

[6] Z. Guo, B. Y. Liaw, X. Qiu, L. Gao, and C. Zhang, "Optimal charging method for lithium ion batteries using a universal voltage protocol accommodating aging," Journal of Power Sources, vol. 274, pp. 957-964, 2015/01/15/ 2015, doi: https://doi.org/10.1016/j.jpowsour.2014.10.185.

[7] T. Ikeya et al., "Multi-step constant-current charging method for an electric vehicle nickel/metal hydride battery with high-energy efficiency and long cycle life," Journal of Power Sources, vol. 105, no. 1, pp. 6-12, 2002/03/05/ 2002, doi: https://doi.org/10.1016/S0378-7753(01)00907-7.
[8] T. Ikeya et al., "Multi-step constant-current charging method for electric vehicle, valve-regulated, lead/acid batteries during night time for load-levelling," Journal of Power Sources, vol. 75, no. 1, pp. 101-107, 1998/09/01/ 1998, doi: https://doi.org/10.1016/S0378-7753(98)00102-5.
[9] R. C. Cope and Y. Podrazhansky, "The art of battery charging," in Fourteenth Annual Battery Conference on Applications and Advances. Proceedings of the Conference (Cat. No.99TH8371), 12-15 Jan. 1999 1999, pp. 233-235, doi: 10.1109/BCAA.1999.795996.
[10] J. Li, E. Murphy, J. Winnick, and P. A. Kohl, "The effects of pulse charging on cycling characteristics of commercial lithium-ion batteries," Journal of Power Sources, vol. 102, no. 1, pp. 302-309, 2001/12/01/ 2001, doi: https://doi.org/10.1016/S0378-7753(01)00820-5.
[11] Y. Liu, C. Hsieh, and Y. Luo, "Search for an Optimal Five-Step Charging Pattern for Li-Ion Batteries Using Consecutive Orthogonal Arrays," IEEE Transactions on Energy Conversion, vol. 26, no. 2, pp. 654-661, 2011, doi: 10.1109/TEC.2010.2103077.
[12] P. H. L. Notten, J. H. G. O. h. Veld, and J. R. G. v. Beek, "Boostcharging Li-ion batteries: A challenging new charging concept," Journal of Power Sources, vol. 145, no. 1, pp. 89-94, 2005/07/04/ 2005, doi: https://doi.org/10.1016/j.jpowsour.2004.12.038.
[13] F. Savoye, P. Venet, M. Millet, and J. Groot, "Impact of Periodic Current Pulses on Li-Ion Battery Performance," IEEE Transactions on Industrial Electronics, vol. 59, no. 9, pp. 3481-3488, 2012, doi: 10.1109/TIE.2011.2172172.
[14] V. Svoboda, H. Doering, and J. Garche, "The influence of fast charging on the performance of VRLA batteries," Journal of Power Sources, vol. 144, no. 1, pp. 244-254, 2005/06/01/ 2005, doi: https://doi.org/10.1016/j.jpowsour.2004.12.026.
[15] S. S. Zhang, "The effect of the charging protocol on the cycle life of a Li-ion battery," Journal of Power Sources, vol. 161, no. 2, pp. 1385-1391, 2006/10/27/ 2006, doi: https://doi.org/10.1016/j.jpowsour.2006.06.040.
[16] P. Keil and A. Jossen, "Charging protocols for lithium-ion batteries and their impact on cycle life—An experimental study with different 18650 high-power cells," Journal of Energy Storage, vol. 6, pp. 125-141, 2016/05/01/ 2016, doi: https://doi.org/10.1016/j.est.2016.02.005.
[17] R. C. B. H. M. Mank, "Modulated, temperature-based multi-CC-CV charging technique for Li-ion/Li-polymer batteries," US Patent US8816648B2, 2009.
[18] C. Brivio, V. Musolino, M. Merlo, and C. Ballif, "A Physically-Based Electrical Model for Lithium-Ion Cells," IEEE Transactions on Energy Conversion, vol. 34, no. 2, pp. 594-603, 2019, doi: 10.1109/TEC.2018.2869272.
[19] T. B. Soeiro and P. Bauer, "Three-Phase DC-Type Isolated Electric Vehicle Charger Featuring Zero Voltage Switching," 2019 AEIT International Conference of Electrical and Electronic Technologies for Automotive (AEIT AUTOMOTIVE), Torino, Italy, 2019, pp. 1-6, doi: 10.23919/EETA.2019.8804550.
[20] M. Stecca, L. R. Elizondo, T. B. Soeiro, P. Bauer and P. Palensky, "A Comprehensive Review of the Integration of Battery Energy Storage Systems Into Distribution Networks," in IEEE Open Journal of the Industrial Electronics Society, vol. 1, pp. 46-65, 2020, doi: 10.1109/OJIES.2020.2981832.
[21] U. Badstübner, "Ultra-High Performance Telecom DC-DC Converter," Ph.D. dissertation, ETH Zurich, Switzerland, 2012.